Research Article
doi.org/10.1002/cbic.202400380
Chemistry Europe
European Chemical Societies Publishing

www.chembiochem.org

Iron-Sulfur Peptides Mimicking Ferredoxin for an Efficient Electron Transfer to Hydrogenase

Umberto Terranova*[a]

In the green alga *Chlamydomonas reinhardtii*, hydrogenase HydA1 converts protons and electrons to H_2 at the H-cluster, which includes a [4Fe–4S] cluster linked to a [2Fe] cluster. The yield of H_2 is limited by the electron transfer to HydA1, mediated by the iron-sulfur unit of a photosynthetic electron transfer ferredoxin (PetF). In this study, I have investigated by molecular dynamics and the hybrid quantum mechanics/molecular mechanics method two canonical iron-sulfur peptides (PM1 and F_BM) that hold potential as PetF replacements. Using a docking approach, I predict that the distance between the two iron-sulfur clusters in F_BM/HydA1 is shorter than in PM1/HydA1, ensuring a greater electron transfer rate. This finding is in line with the reported higher H_2 production rates for F_BM/HydA1. I also show that the redox potential of these peptides, and therefore their electron transfer properties, can be changed by single-residue mutations in the secondary coordination sphere of their cluster. In particular, I have designed a PM1 variant that disrupts the hydrogen-bonding network between water and the cluster, shifting the redox potential negatively compared to PM1. These results will guide experiments aimed at replacing PetF with peptides that can unlock the biotechnological potential of the alga.

Introduction

Iron-sulfur enzymes are promising candidates as biocatalysts to decarbonise our energy production.[1–5] Microalgae such as *Chlamydomonas reinhardtii* use hydrogenase HydA1 (as well as the variant HydA2) to catalyse the reduction of protons to H_2 and dispose of any excess reducing power.[6–9] The reaction occurs at the so-called H-cluster, which consists of a [4Fe–4S] cluster and a [2Fe] cluster (coordinated with CO, CN and dithiolate ligands) bridged by a cysteine.[10] HydA1 receives the electrons from a photosynthetic electron transfer ferredoxin (PetF) containing a [2Fe–2S] cluster where each Fe atom is tetrahedrally coordinated to four S atoms (two from the cluster and two from two nearby cysteines).[11] The [2Fe–2S] cluster of PetF typically cycles between a +2 oxidised ($Fe^{3+}Fe^{3+}$) and a +1 reduced ($Fe^{2+}Fe^{3+}$) state, with both Fe ions antiferromagnetically coupled.[12]

In addition to HydA1, PetF partners with other enzymes, among which ferredoxin-$NADP^+$ reductase,[13] nitrite reductase[14] and ferredoxin-thioredoxin reductase,[15] in alternative metabolic pathways that limit the H_2 production. Solutions that re-engineer the PetF/HydA1 interface to redirect the flow of electrons to HydA1 could then open the way to a novel class of cellular biocatalysts. However, increasing the affinity towards HydA1 by exploring PetF variants is challenging, as most of the PetF residues at the interface with HydA1 interact also with the competing enzymes above.[16,17] In this scenario, the replacement of PetF with artificial proteins that preferentially bind and donate their electrons to HydA1 appears attractive.

Significant literature exists on the *de novo* design of iron-sulfur peptides.[18–22] Antonkine *et al.* have successfully incorporated a [4Fe–4S] cluster into two 16-amino acid peptide maquettes (F_AM and F_BM) derived from the sequence of Photosystem I, as confirmed by UV-vis, electron paramagnetic resonance (EPR) and Mössbauer spectroscopies.[23] The [4Fe–4S] cluster can adopt either an oxidised +2 ($2Fe^{2+}$ $2Fe^{3+}$) or a reduced +1 ($3Fe^{2+}$ $1Fe^{3+}$) state. Also in this case, antiferromagnetic coupling between ion pairs is present. More recently, Gunzel *et al.* have synthesised a 22-amino acid peptide maquette (PM1), based on the sequence of *C. reinhardtii* PetF, that contains a [2Fe–2S] cluster.[24] While EPR and/or Mössbauer spectroscopy evidence are not available yet, the reported UV-vis spectra indicates cluster formation. The same authors have shown that both F_BM and PM1 are able to reduce HydA1, which results into H_2 production *in vitro*.[24] For *in vivo* applications, however, adjustments to the peptide sequence might be required to ensure reduction by Photosystem I of *C. reinhardtii* (some evidence suggests that F_BM can bind Photosystem I).[23]

Detailed knowledge of the interface is crucial to improve the electron transfer between two biomolecules.[25] Rumpel *et al.* have suggested a model of the PetF/HydA1 complex based on docking simulations,[12] while kinetic measurements of H_2 production with several PetF and HydA1 variants[17] have provided key information on the residues at the interface, including the identification of mutations able to affect the H_2 production.[17,26,27]

In addition to surface complementarity, an efficient electron transfer requires that the redox potentials of the two molecular complexes are suitably aligned.[28] Given their large number of

[a] *Dr. U. Terranova*
Faculty of Medicine and Health Sciences, University of Buckingham, Crewe Campus, Crewe, CW1 5DU, UK
E-mail: umberto.terranova@buckingham.ac.uk

Supporting information for this article is available on the WWW under https://doi.org/10.1002/cbic.202400380

© 2024 The Authors. ChemBioChem published by Wiley-VCH GmbH. This is an open access article under the terms of the Creative Commons Attribution License, which permits use, distribution and reproduction in any medium, provided the original work is properly cited.

© 2024 The Authors. ChemBioChem published by Wiley-VCH GmbH

partners in nature, it is not surprising that ferredoxins can cover a remarkable redox potential range of 0.8 V by modulating the environment around the cluster, *i.e.* Fe ligands, secondary shell and hydrogen-bond network.[29] It is therefore important to find strategies that can fine-tune the redox potential of the *de novo* designed peptide, which should ideally match that of HydA1.

Here, I combine molecular dynamics (MD) with docking simulations to predict models of F_BM and PM1 at the interface with HydA1. I find that the F_BM/HydA1 complex is particularly suitable for an efficient electron transfer, thanks to the short distance between the iron-sulfur clusters of the two biomolecules. The residues at the interface engage in a stable binding. In addition, I introduce an amino acid mutation in the second coordination sphere of PM1, i.e. the replacement of a leucine with a bulkier phenylalanine, that shifts the peptide redox potential negatively, as shown by quantum mechanics/molecular mechanics (QM/MM) calculations. This approach can be used to fine-tune the redox potential of other iron-sulfur peptides.

Results and Discussion

Peptide Binding to Hydrogenase

During the 0.5 ns production run, 10 peptide configurations spaced at 50 ps intervals were extracted and used as input ligands in ZDOCK.[30] The top 10 docking predictions were selected for each configuration, for a total of 100 peptide/protein complexes analysed.

Figure 1 shows the histograms of the distances between the [4Fe–4S] cluster of HydA1 and the iron-sulfur clusters of both peptides. All 100 PM1 geometries have an intercluster distance (measured centre-to-centre) larger than 25 Å. Among the PM1/HydA1 complexes with distances between 25 and 30 Å, the one that was scored highest by ZDOCK is shown in the upper panel of Figure 2. Similarly large distances are compatible with electron transfer between proteins (possibly facilitated by a hopping mechanism), as observed for example in mixed-metal hemoglobins.[31] The F_BM distribution spreads across a wider range, extending to values as small as 7 Å. In particular, while a large distance of 31 Å is observed in the top structure returned by ZDOCK, the second-ranked structure features a significantly shorter intercluster distance of 13 Å. This value is comparable to the typical 14 Å distance found between iron-sulfur clusters functioning as electron transfer chains in hydrogenases.[32] The shorter distance between the redox centres of F_BM/HydA1, compared to PM1/HydA1, ensures a greater electron transfer rate according to Marcus theory,[33] and is in line with the larger H_2 production reported *in vitro*.[24] Thus, the rest of this section will focus on this F_BM/HydA1 structure, which I illustrate in the lower panel of Figure 2. It is worth noting, though, that other configurations with lower ZDOCK scores may also contribute to the electron transfer.

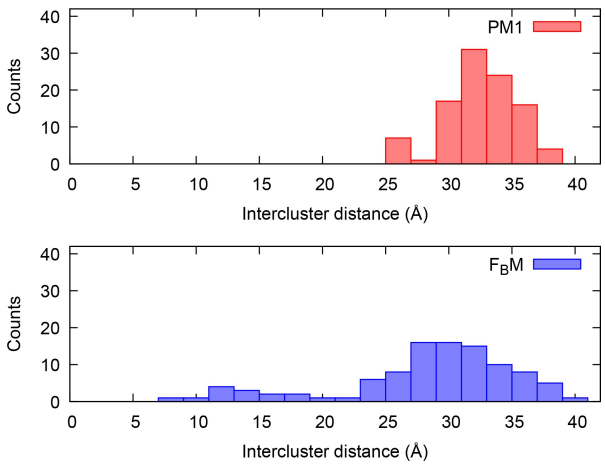


Figure 1. Intercluster distances for the top 100 F_BM/HydA1 and PM1/HydA1 complexes predicted by ZDOCK.

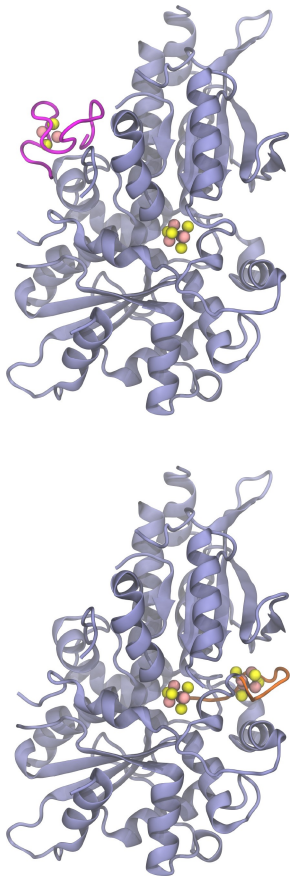


Figure 2. Docking structure of PM1/HydA1 (upper panel) and F_BM/HydA1 (lower panel). Notice the proximity between the two clusters in F_BM/HydA1. Colour code: HydA1 – violet, PM1 – magenta, F_BM – orange, Fe – pink, S – yellow, C – cyan, N – blue.

The stability of the complex was tested over 4 ns of MD, during which the peptide remained docked to the initial pocket. The trajectory overlay of Figure 3 shows little residue fluctuations, with the exception of some rearrangement around the cluster occurring during the first ns of equilibration.

The upper panel of Figure 4 shows that the intercluster distance *d* stabilises at about 14 Å. The mid panel of Figure 4

© 2024 The Authors. ChemBioChem published by Wiley-VCH GmbH

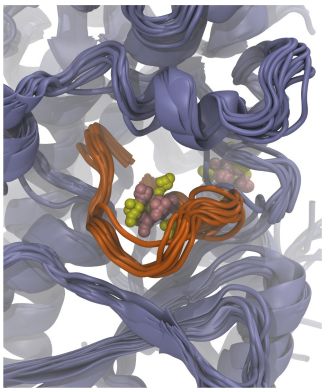


Figure 3. Trajectory overlay of the F_BM/HydA1 complex. Colour code: HydA1 – violet, F_BM – orange, Fe – pink, S – yellow.

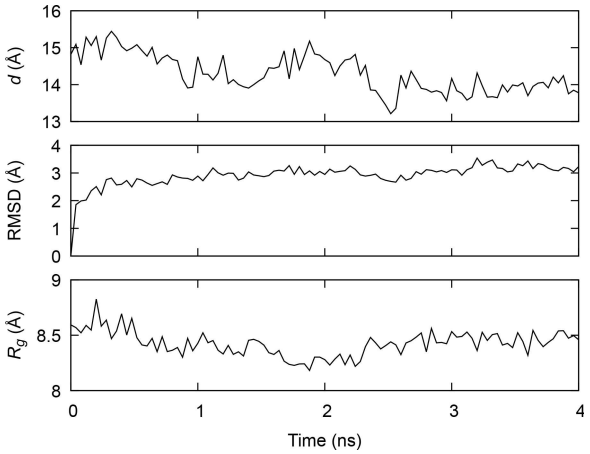


Figure 4. Intercluster distance (*d*, upper panel), root mean square displacement (RMSD, mid panel) and radius of gyration (R_g, lower panel) of F_BM during the 4 ns trajectory.

illustrates the root mean square deviation (RMSD) of F_BM, which measures the difference from the initial structure:

$$\mathrm{RMSD} = \sqrt{\frac{1}{N}\sum_{i=1}^{N}|r_i(t) - r_i(0)|^2} \quad (1)$$

where N is the number of atoms and $r_i(t)$ are the coordinates of atom i at time t. It can be observed that the RMSD converges to about 3 Å already within the first ns of trajectory. The lower panel of Figure 4 shows the radius of gyration (R_g), which measures the distance of the atoms from their centre of mass:

$$R_g = \sqrt{\frac{1}{M}\sum_{i=1}^{N} m_i|r_i(t) - r_{\mathrm{cm}}(t)|^2} \quad (2)$$

where M is the mass of the peptide and r_{cm} the position of its centre of mass. Oscillations of R_g are within a narrow interval of about 0.5 Å. All trends above confirm the stability of the predicted F_BM/HydA1 interface.

Figure 5 depicts the interface corresponding to the last snapshot of MD. While residues of HydA1 such as Thr252, Thr253 and Gln400 are involved in important hydrogen bonds with F_BM, Lys288 is particularly crucial for the stability of the complex. In addition to forming a hydrogen bond with Thr8, its NH_3^+ group interacts directly with a S^{2-} ion of the [4Fe–4S] cluster of F_BM, while also forming a salt bridge with Glu13. I summarise all interactions occurring at a distance below 3 Å between non-hydrogen atoms in Table 1. It is significant that none of the HydA1 residues mentioned above are relevant for the interface with PetF.[12]

Tuning the Redox Potential

The capability to fine-tune the redox potential of a partner molecule is important to modulate the thermodynamic driving force for electron transfer (see Eq. (4)). In addition, the redox potential directly affects the electron transfer rate.[34] In this section, I will demonstrate that shielding the iron-sulfur cluster from water decreases its redox potential, in line with previous studies.[34,35] I will focus on PM1, whose conformation during MD was particularly suitable for illustrating this effect. However, this strategy is general and could be extended to other iron-sulfur peptides.

The upper panel of Figure 6 illustrates the last MD snapshot of PM1 in the reduced state. While the [2Fe–2S] cluster is surrounded by several residues, little shielding is offered by

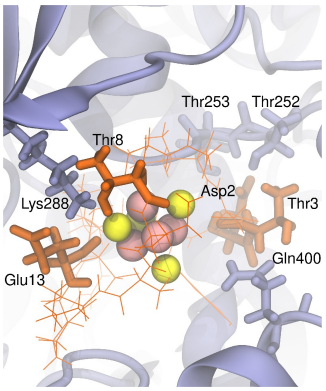


Figure 5. Interface of the F_BM/HydA1 complex taken during the last snapshot of MD. The most relevant residues have been labelled. Colour code: HydA1 – violet, F_BM – orange, Fe – pink, S – yellow.

Table 1. Interactions between F_BM and HydA1 at a distance below 3 Å between any two non-hydrogen atoms.

F_BM residue	HydA1 residue	Type	Groups (F_BM···HydA1)
Asp2	Thr252	hydrogen bond	COO^-···H–O
Asp2	Thr253	hydrogen bond	COO^-···H–N
Thr3	Gln400	hydrogen bond	O–H···CO
Thr8	Lys288	hydrogen bond	CO···H–N
Glu13	Lys288	salt bridge	COO^-···NH_3^+
[4Fe-4S]	Lys288	ionic	S^{2-}···NH_3^+

© 2024 The Authors. ChemBioChem published by Wiley-VCH GmbH

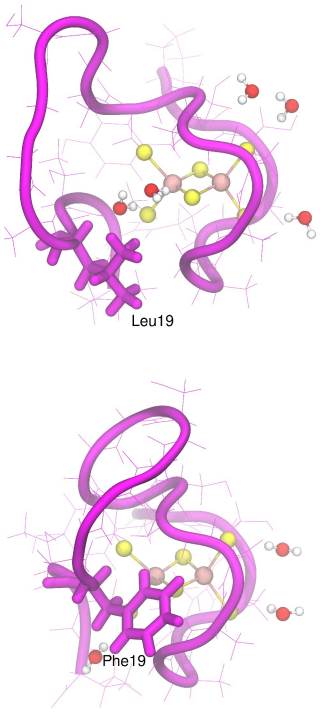


Figure 6. MD snapshots of PM1 (upper panel) and PM1-L19F (lower panel) showing all water molecules at a distance less than 3.7 Å from the [2Fe–2S] cluster. Colour code: PM1 – magenta, Fe – pink, S – yellow, O – red, H – white.

Leu19, and five water molecules have accessed the cluster to form hydrogen bonds with the S^{2-} ions. Using a O–S distance of 3.7 Å, and a O–H–S angle of 40° as a cutoff for the hydrogen bond criterion,[36] 3.5 hydrogen bonds formed on average between water and the cluster during the trajectory. Similar conclusions can be drawn for the oxidised state, with 1.5 hydrogen bonds formed on average.

One way to lower the redox potential of iron-sulfur proteins (by tens of mV) is by eliminating the hydrogen bonds formed by the cluster with its surrounding residues, as this destabilises the reduced more than the oxidised state.[34,37] I reasoned that replacing the leucine with a bulkier amino acid such as phenylalanine should shield more the cluster from water. Disrupting the hydrogen-bonding network should then lower the redox potential of the peptide. For this reason, I designed a PM1 variant with the Leu19 to Phe19 substitution, PM1-L19F hereafter. Structures with both +2 and +1 cluster oxidation states were solvated and equilibrated for 1 ns, using an identical protocol to that of the original PM1 peptide.

The bottom panel of Figure 6 illustrates the last MD snapshot of PM1-L19F in the reduced state. As speculated, the introduced phenyl group is effective in preventing water from accessing the cluster (only three water molecules are now in proximity of the cluster). In addition to the larger side chain, the L19F mutation increases the hydrophobicity of the corresponding portion of the peptide, contributing to a tighter packing around the [2Fe–2S] cluster. This trend is captured by the comparison between R_g of both peptides reported in Figure 7, which clearly indicates that PM1-L19F is more compact than

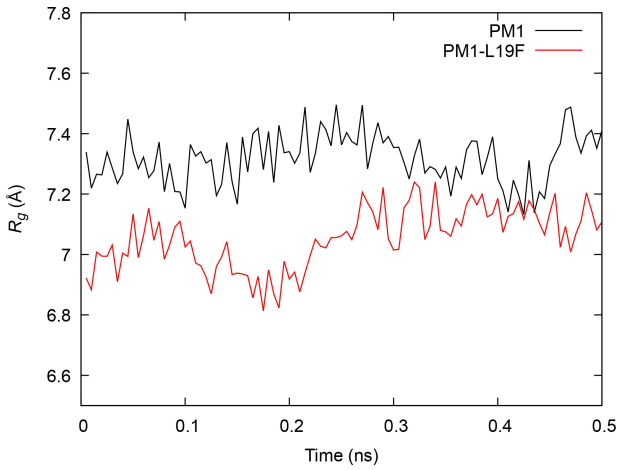


Figure 7. Radius of gyration of PM1 and PM1-L19F during the MD trajectory.

PM1. As a consequence, the average number of hydrogen bonds formed between water and the [2Fe–2S] cluster decreases from 3.5 to 2.3 (about 34%). The corresponding change in the oxidised state is from 1.5 to 1.2 (about 20%), confirming that shielding the cluster from water disrupts the hydrogen-bonding network in the reduced state more significantly than in the oxidised. In line with these results, inaccessibility to water destabilises the +1 state of high-potential iron-sulfur proteins, making the +2/+3 couple accessible.[29,38]

Figure 8 shows the QM/MM vertical energy gaps ΔE of PM1 and PM1-L19F, in the reduced and oxidised state, for the selected 100 snapshots of classical MD. Energy gaps fluctuate around an average value, confirming the systems are well equilibrated. Some QM/MM energies were difficult to converge. The corresponding points appear as outliers, but they do not influence qualitatively the results. Using Eqs. (4) and (8), I obtained a redox potential of −0.04 V for PM1. This value is higher than that of about −0.4 V measured for PetF.[39] I emphasise that the accurate calculations of redox potentials remain a challenge. They involve a change in the total charge

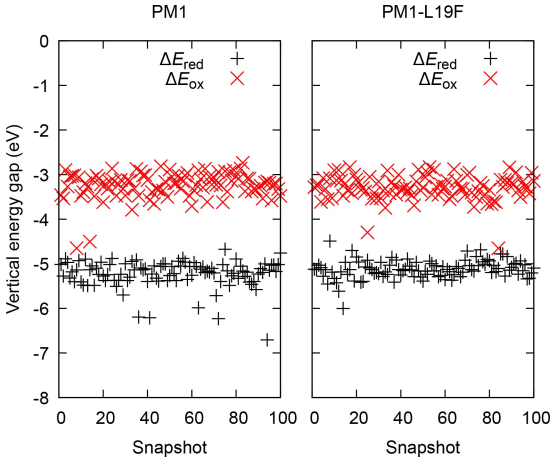


Figure 8. Vertical energy gaps of PM1 and PM1-L19F in the reduced and oxidised state.

© 2024 The Authors. ChemBioChem published by Wiley-VCH GmbH

of the system (see subsection "Calculating the Redox Potential"), and it is well known that electrostatic interactions decay slowly within proteins.[40] For example, the density functional theory (DFT) calculated redox potential of ferredoxin I from *D. africanus* and that of a Rieske iron-sulfur protein resulted about 0.3 V lower than experiment.[41,42] However, the same studies reported a high accuracy in the calculation of relative redox potentials of different proteins or at different pH, in line with typical errors on the order of 0.01 V,[40] making our comparison between PM1 and PM1-L19F meaningful. For the latter, we calculated a redox potential of −0.08 V, i.e. 0.04 V more negative than PM1. At this point, it is important to consider that (i) the shift in the redox potential occurred for the isolated peptides, but binding to HydA1 can further affect the redox potential; (ii) the reorganisation energy could change in the mutated peptide, affecting the rate of electron transfer, particularly with the differences in solvent exposure and structures shown in Figure 6. However, while we should exert caution in the quantitative interpretation of the DFT value, the observed shift suggests that the degree of shielding of the iron-sulfur cluster from water could be a valuable parameter to modulate the redox potential of these peptides.

Conclusions

I have presented a combined MD/docking investigation of the interfaces between two well-known iron-sulfur peptides (PM1 and F_BM) and HydA1 from the green alga *C. reinhardtii*. Both peptides have recently been found to mimic *in vitro* the electron transfer role of natural PetF proteins, which motivated me to explore them further. Even by binding HydA1 at a different area than PetF, F_BM, at odds with PM1, is at a favourable position for electron transfer, thanks to its stable interaction and short intercluster distance. Another key outcome from this study is a strategy that successfully lowers the redox potential of PM1 (or any other iron-sulfur peptide), based on the principle that hydrogen bonds between water and the [2Fe–2S] cluster stabilise the reduced more than the oxidised state. I suggested a PM1-L19F variant that, being more hydrophobic than PM1, allows less water molecules to access the cluster. While the search for novel peptides able to outperform PetF remains open, these results are a valuable step in that direction.

Computational Methods

Modelling the Peptide/Protein Complex

The peptide/protein complexes were modelled by the docking programme ZDOCK,[30] using its score function to evaluate all possible interactions of the peptides while keeping fixed the protein. As HydA1 structures with a complete H-cluster from *C. reinhardtii* are not currently available, the HydA1 used in this study (PDB code 3lx4) includes only the [4Fe–4S] cluster, while presenting an open pocket in correspondence of the [2Fe] cluster. This structure has already been used to derive a docking model for the binding of PetF to HydA1,[12] as only minor structural adjustments are expected upon enzyme maturation.[43]

Ten geometries, extracted every 50 ps of the 0.5 ns MD trajectory in the reduced state, were used for both peptides, following the procedure outlined below. To model PM1 (sequence PYSCRAGACSSCAGSGGALTCV), I inserted a SGGA loop in-between the PYSCRAGACSSCAG and LTCV fragments of the PetF with PDB code 6kv0. The initial coordinates of F_BM (sequence YDTCIGCTQCKPECPW) were generated by introducing the KPE loop in-between the YDTCIGCTQC and CP (with an additional W residue) sequences of Photosystem I with PDB code 1jb0. To create the loops, fragments were extended with residues from the original structure that were subsequently converted by the Mutator Plugin of VMD[44] to the desired loop residues. Where necessary, residues were graphically translated/rotated using VMD to enable the loop to join the two fragments. All missing hydrogen atoms were added with VMD. In both peptides, the iron-sulfur clusters were ligated to four cysteines as in their protein of reference. Both a reduced and an oxidised species of each peptide were generated, which were then solvated in a cubic water box with a padding of 15 Å. Sodium ions were added to ensure charge neutrality. The simulation boxes of the reduced (oxidised) PM1 and F_BM models contained respectively 10235 (10237) and 11438 (11440) atoms. Solvent and peptides were optimised by 2000 steps of a limited memory algorithm (LBFGS)[45] while fixing all the Cartesian coordinates of the iron-sulfur clusters to their initial positions. Prior to the 0.5 ns production run, the systems were equilibrated for 1 ns, which proved sufficient to converge the RMSD of both solvated peptides.

Calculating the Redox Potential

I have calculated the standard redox potential of the iron-sulfur clusters by using the linear response approximation (LRA) within the thermodynamic integration method.[46–48] The standard redox potential E° for a reaction transferring n moles of electrons:

$$\mathrm{ox} + ne^- \rightleftharpoons \mathrm{red} \tag{3}$$

is related to the standard Gibbs free energy change ΔG° by:

$$E^\circ = -\frac{\Delta G^\circ}{nF} - E^\circ_{\mathrm{SHE}} \tag{4}$$

where F is the Faraday constant and E°_{SHE} the absolute potential of the standard hydrogen electrode ($E^\circ_{\mathrm{SHE}} = 4.24$ V in Ref. [49]).

Under the assumption that the pV term is negligible,[50,51] G can be replaced by the Helmholtz free energy A. At this point, the parameter λ connecting adiabatically the oxidised ($\lambda = 0$) to the reduced ($\lambda = 1$) state is introduced and the potential energy of the system written as function of λ:

$$E(\lambda) = \lambda E_{\mathrm{red}} + (1-\lambda)E_{\mathrm{ox}} \tag{5}$$

while also noting that:[52]

$$\frac{\partial A}{\partial \lambda} = \left\langle \frac{\partial E}{\partial \lambda} \right\rangle \tag{6}$$

Making use of Eqs. (5) and (6), ΔA can be calculated by integrating the average vertical energy gaps $\langle E_{\mathrm{red}} - E_{\mathrm{ox}} \rangle$:

© 2024 The Authors. ChemBioChem published by Wiley-VCH GmbH

$$\Delta A = \int_0^1 d\lambda \frac{\partial A}{\partial \lambda} = \int_0^1 d\lambda \left\langle \frac{\partial E}{\partial \lambda} \right\rangle = \int_0^1 d\lambda \langle E_{red} - E_{ox} \rangle = \int_0^1 d\lambda \langle \Delta E \rangle \quad (7)$$

In the LRA, the free energy derivative term is assumed to be linear in λ, so that the integral can be calculated using only the initial and final state:

$$\Delta A = \frac{1}{2}(\langle \Delta E \rangle_{red} + \langle \Delta E \rangle_{ox}) \quad (8)$$

where the vertical energy gaps, averaged over the configurations, are evaluated at the geometry of the reduced and oxidised systems.

Simulation Details

All atomistic simulations were performed with CP2K.[53] The molecular mechanics interactions were modelled by the CHARMM36 force field,[54] which includes a slightly modified TIP3P water model.[55] Parameters for the iron-sulfur clusters were taken from the work by Chang *et al.*[56] A cutoff radius of 12 Å was used for all nonbonded interactions. All MD simulations were performed in the NPT ensemble[57] at a temperature of 300 K and a pressure of 1 bar. The time step corresponded to 1 fs.

Both vertical energy gaps ΔE of Eq. (8) were calculated at the QM/MM level by CP2K (without reoptimising geometries), using 100 configurations spaced at 5 ps intervals and obtained from the 0.5 ns MD trajectories. A similar approach has been adopted in other studies.[58] The peptide represented the QM region that I treated by DFT. I employed the PBE exchange-correlation functional,[59] the DZVP-MOLOPT basis set,[60] and the GTH pseudopotentials proposed by Goedecker, Teter and Hutter.[61] This combination of functional and basis set has been successfully used in previous DFT studies of both the hydrogen-bond network of hydrogenase[62] and the mimics of its H-cluster.[63] It balances the accuracy and efficiency required for this work. Calculations used a plane-wave cutoff of 400 Ry and a target accuracy for the self-consistent field convergence of 1.0×10^{-5}. Electrostatic interactions between the QM and MM regions were handled by Gaussian expansion of the electrostatic potential (GEEP).[64] The antiferromagnetic coupling of the Fe atoms was treated by the broken symmetry approach implemented in CP2K, which enables the input of the desired distribution of electrons across the alpha and beta d-orbitals of each Fe atom. DFT energies are only marginally affected by the antiferromagnetic coupling scheme.[65]

Acknowledgements

Via membership of the UK's HEC Materials Chemistry Consortium, which is funded by EPSRC (EP/R029431 and EP/X035859), this work used the ARCHER2 UK National Supercomputing Service (http://www.archer2.ac.uk).

Conflict of Interests

The authors declare no conflict of interest.

Data Availability Statement

The data that support the findings of this study are available in the supplementary material of this article.

Keywords: iron-sulfur peptides · hydrogenase · ferredoxin · molecular dynamics · QM/MM

[1] J. G. Rebelein, M. T. Stiebritz, C. C. Lee, Y. Hu, *Nat. Chem. Biol.* **2017**, *13*, 147.
[2] C. C. Lee, M. T. Stiebritz, Y. Hu, *Acc. Chem. Res.* **2019**, *52*, 1168.
[3] D. Tombolelli, M. A. Mroginski, *J. Phys. Chem. B* **2019**, *123*, 3409.
[4] U. Terranova, *JBIC J. Biol. Inorg. Chem.* **2021**, *26*, 617.
[5] J. Ruickoldt, Y. Basak, L. Domnik, J.-H. Jeoung, H. Dobbek, *ACS Catal.* **2022**, *12*, 13131.
[6] M. L. Ghirardi, L. Zhang, J. W. Lee, T. Flynn, M. Seibert, E. Greenbaum, A. Melis, *Trends Biotechnol.* **2000**, *18*, 506.
[7] M. L. Ghirardi, M. C. Posewitz, P.-C. Maness, A. Dubini, J. Yu, M. Seibert, *Annu. Rev. Plant Biol.* **2007**, *58*, 71.
[8] M. Oey, A. L. Sawyer, I. L. Ross, B. Hankamer, *Plant Biotechnol. J.* **2016**, *14*, 1487.
[9] L. Wei, W. Ma, *GCB Bioenergy* **2024**, *16*, e13118.
[10] L. Kertess, A. Adamska-Venkatesh, P. Rodríguez-Maciá, O. Rüdiger, W. Lubitz, T. Happe, *Chem. Sci.* **2017**, *8*, 8127.
[11] J. Couturier, B. Touraine, J.-F. Briat, N. Rouhier, *Front. Plant Sci.* **2013**, *4*, 56243.
[12] S. Rumpel, J. F. Siebel, M. Diallo, C. Farès, E. J. Reijerse, W. Lubitz, *ChemBioChem* **2015**, *16*, 1663.
[13] G. Kurisu, M. Kusunoki, E. Katoh, T. Yamazaki, K. Teshima, Y. Onda, Y. Kimata-Ariga, T. Hase, *Nat. Struct. Mol. Biol.* **2001**, *8*, 117.
[14] M. Hirasawa, J. N. Tripathy, R. Somasundaram, M. K. Johnson, M. Bhalla, J. P. Allen, D. B. Knaff, *Mol. Plant Pathol.* **2009**, *2*, 407.
[15] S. Dai, R. Friemann, D. A. Glauser, F. Bourquin, W. Manieri, P. Schürmann, H. Eklund, *Nature* **2007**, *448*, 92.
[16] A. Sawyer, M. Winkler, *Photosynth. Res.* **2017**, *134*, 307.
[17] M. Winkler, S. Kuhlgert, M. Hippler, T. Happe, *J. Biol. Chem.* **2009**, *284*, 36620.
[18] B. R. Gibney, S. E. Mulholland, F. Rabanal, P. L. Dutton, *Proc. Natl. Acad. Sci. USA* **1996**, *93*, 15041.
[19] S. E. Mulholland, B. R. Gibney, F. Rabanal, P. L. Dutton, *J. Am. Chem. Soc.* **1998**, *120*, 10296.
[20] S. E. Mulholland, B. R. Gibney, F. Rabanal, P. L. Dutton, *Biochemistry* **1999**, *38*, 10442.
[21] J. D. Kim, D. H. Pike, A. M. Tyryshkin, G. Swapna, H. Raanan, G. T. Montelione, V. Nanda, P. G. Falkowski, *J. Am. Chem. Soc.* **2018**, *140*, 11210.
[22] A. Bombana, M. Shanmugam, D. Collison, A. J. Kibler, G. N. Newton, C. M. Jäger, A. K. Croft, S. Morra, N. J. Mitchell, *ChemBioChem* **2023**, *24*, e202300250.
[23] M. L. Antonkine, M. S. Koay, B. Epel, C. Breitenstein, O. Gopta, W. Gärtner, E. Bill, W. Lubitz, *Biochim. Biophys. Acta Bioenerg.* **2009**, *1787*, 995.
[24] A. Günzel, V. Engelbrecht, T. Happe, *JBIC J. Biol. Inorg. Chem.* **2022**, *27*, 631.
[25] C. H. Chang, P. W. King, M. L. Ghirardi, K. Kim, *Biophys. J.* **2007**, *93*, 3034.
[26] M. Winkler, A. Hemschemeier, J. Jacobs, S. Stripp, T. Happe, *Eur. J. Cell Biol.* **2010**, *89*, 998.
[27] M. Boehm, M. Alahuhta, D. W. Mulder, E. A. Peden, H. Long, R. Brunecky, V. V. Lunin, P. W. King, M. L. Ghirardi, A. Dubini, *Photosynth. Res.* **2016**, *128*, 45.
[28] H. Long, C. H. Chang, P. W. King, M. L. Ghirardi, K. Kim, *Biophys. J.* **2008**, *95*, 3753.
[29] J. Liu, S. Chakraborty, P. Hosseinzadeh, Y. Yu, S. Tian, I. Petrik, A. Bhagi, Y. Lu, *Chem. Rev.* **2014**, *114*, 4366.
[30] B. G. Pierce, K. Wiehe, H. Hwang, B.-H. Kim, T. Vreven, Z. Weng, *Bioinformatics* **2014**, *30*, 1771.
[31] H. B. Gray, J. R. Winkler, *Proc. Natl. Acad. Sci. USA* **2005**, *102*, 3534.
[32] C. Furlan, N. Chongdar, P. Gupta, W. Lubitz, H. Ogata, J. N. Blaza, J. A. Birrell, *eLife* **2022**, *11*, e79361.
[33] J. Hopfield, *Proc. Natl. Acad. Sci. USA* **1974**, *71*, 3640.
[34] P. Hosseinzadeh, Y. Lu, *Biochim. Biophys. Acta Bioenerg.* **2016**, *1857*, 557.
[35] G. Jensen, A. Warshel, P. Stephens, *Biochemistry* **1994**, *33*, 10911.

© 2024 The Authors. ChemBioChem published by Wiley-VCH GmbH

[36] U. Terranova, N. H. de Leeuw, *Phys. Chem. Chem. Phys.* **2014**, *16*, 13426.
[37] E. Denke, T. Merbitz-Zahradnik, O. M. Hatzfeld, C. H. Snyder, T. A. Link, B. L. Trumpower, *J. Biol. Chem.* **1998**, *273*, 9085.
[38] G. Backes, Y. Mino, T. M. Loehr, T. E. Meyer, M. A. Cusanovich, W. V. Sweeney, E. T. Adman, J. Sanders-Loehr, *J. Am. Chem. Soc.* **1991**, *113*, 2055.
[39] M. Heghmanns, A. Günzel, D. Brandis, Y. Kutin, V. Engelbrecht, M. Winkler, T. Happe, M. Kasanmascheff, *Biophys. Rep.* **2021**, *1*, 100016.
[40] S. Jafari, Y. A. Tavares Santos, J. Bergmann, M. Irani, U. Ryde, *Inorg. Chem.* **2022**, *61*, 5991.
[41] R. A. Torres, T. Lovell, L. Noodleman, D. A. Case, *J. Am. Chem. Soc.* **2003**, *125*, 1923.
[42] M. G. Ullmann, L. Noodleman, D. A. Case, *JBIC J. Biol. Inorg. Chem.* **2002**, *7*, 632.
[43] A. S. Pandey, T. V. Harris, L. J. Giles, J. W. Peters, R. K. Szilagyi, *J. Am. Chem. Soc.* **2008**, *130*, 4533.
[44] W. Humphrey, A. Dalke, K. Schulten, *J. Mol. Graphics* **1996**, *14*, 33.
[45] R. H. Byrd, P. Lu, J. Nocedal, C. Zhu, *SIAM J. Sci. Comput.* **1995**, *16*, 1190.
[46] J. Blumberger, I. Tavernelli, M. L. Klein, M. Sprik, *J. Chem. Phys.* **2006**, *124*.
[47] G. Hong, D. M. Ivnitski, G. R. Johnson, P. Atanassov, R. Pachter, *J. Am. Chem. Soc.* **2011**, *133*, 4802.
[48] V. Vaissier, T. Van Voorhis, *J. Chem. Theory Comput.* **2016**, *12*, 5111.
[49] A. A. Isse, A. Gennaro, *J. Phys. Chem. B* **2010**, *114*, 7894.
[50] R. Jono, Y. Tateyama, K. Yamashita, *Phys. Chem. Chem. Phys.* **2015**, *17*, 27103.
[51] E. Falbo, T. Penfold, *J. Phys. Chem. C* **2020**, *124*, 15045.
[52] L.-P. Wang, T. Van Voorhis, *J. Chem. Theory Comput.* **2012**, *8*, 610.
[53] T. D. Kühne, M. Iannuzzi, M. Del Ben, V. V. Rybkin, P. Seewald, F. Stein, T. Laino, R. Z. Khaliullin, O. Schütt, F. Schiffmann, et al., *J. Chem. Phys.* **2020**, *152*, 194103.
[54] J. Huang, S. Rauscher, G. Nawrocki, T. Ran, M. Feig, B. L. De Groot, H. Grubmüller, A. D. MacKerell Jr, *Nat. Methods* **2017**, *14*, 71.
[55] W. L. Jorgensen, J. Chandrasekhar, J. D. Madura, R. W. Impey, M. L. Klein, *J. Chem. Phys.* **1983**, *79*, 926.
[56] C. H. Chang, K. Kim, *J. Chem. Theory Comput.* **2009**, *5*, 1137.
[57] W. G. Hoover, *Phys. Rev. A* **1985**, *31*, 1695.
[58] M. Alfonso-Prieto, H. Oberhofer, M. L. Klein, C. Rovira, J. Blumberger, *J. Am. Chem. Soc.* **2011**, *133*, 4285.
[59] J. P. Perdew, K. Burke, M. Ernzerhof, *Phys. Rev. Lett.* **1996**, *77*, 3865.
[60] J. VandeVondele, J. Hutter, *J. Chem. Phys.* **2007**, *127*.
[61] S. Goedecker, M. Teter, J. Hutter, *Phys. Rev. B* **1996**, *54*, 1703.
[62] R. C. Puthenkalathil, B. Ensing, *J. Phys. Chem. B* **2022**, *126*, 403.
[63] R. C. Puthenkalathil, M. Etinski, B. Ensing, *Phys. Chem. Chem. Phys.* **2020**, *22*, 10447.
[64] T. Laino, F. Mohamed, A. Laio, M. Parrinello, *J. Chem. Theory Comput.* **2005**, *1*, 1176.
[65] R.-Z. Liao, P. E. Siegbahn, *Inorg. Chem.* **2019**, *58*, 7931.

Manuscript received: April 24, 2024
Revised manuscript received: July 10, 2024
Accepted manuscript online: July 10, 2024
Version of record online: October 4, 2024

© 2024 The Authors. ChemBioChem published by Wiley-VCH GmbH